Journal of Circuits, Systems, and Computers
Vol. 29, No. 4 (2020) 2050055 (30 pages)

DOI: 10.1142/S0218126620500553

Emulating the Statistical Properties of Indoor Power Line Colored Background Noise for Development of a Power Line Noise Simulator*

Rubi Baishya and Banty Tiru†

Department of Physics, Gauhati University, Guwahati 781014, Assam, India
†*banty_tiru@rediffmail.com*

Utpal Sarma

Department of Instrumentation and USIC, Gauhati University, Guwahati 781014, Assam, India

Received 29 March 2017
Accepted 18 April 2019
Published 21 June 2019

This paper deals with the development of a realistic power line channel simulator wherein power line communication devices can be tested before implementation to meet the massive need of data transfer. The statistics of the noise follow the experimentally observed in different sites, namely the time-varying non-white power spectral densities (PSDs) of the background noise and a target non Gaussian amplitude distribution. The procedure based on the inverse cumulative distribution function method of generation of random numbers and iteratively updating a target spectrum necessitates knowledge of a maximum of 17 parameters for successful implementation and has been validated for three sites in the low-frequency (<500 kHz) and high-frequency (1–30 MHz) bands. The average percentage errors in prediction of the mean of the channel capacity (CC) are 12.68% and 10.66% in the two bands, respectively. The minimum correlations of the distribution of BER of OFDM in a channel corrupted by the simulated and observed noises are is 0.883 and 0.801 in the two bands which are high compared to 0.422 and 0.355, respectively, when the requirement of a target amplitude distribution is neglected. With low-frequency noise emulated by a data acquisition card, an average percentage error of 11.82% in the CC and a correlation of 0.867 (against 0.498) in BER are obtained. The noise thus generated can be used as a testbed for system testing, instead of the conventional static models (additive white Gaussian noise or with time-invariant colored PSD), leading to better optimization of the implemented devices.

Keywords: Power line communication; colored background noise; noise simulation; probability distribution; power spectral density; channel capacity.

*This paper was recommended by Regional Editor Masakazu Sengoku.
†Corresponding author.

1. Introduction

One of the preliminary requirements of implementing a communication system is developing a channel simulator where it can be tested. An efficient simulator takes into account all the variability to replicate closely the observed. This is more so for power line communication (PLC) that uses the available power line (PL) for data transfer. The PLC can be used exclusively or as component of a hybrid communication system,[1–3] in a wide range of low and high bit rate requirements in control, *in-house* and *access* applications like home/office/vehicle automation, smart grids, remote metering,[1,2] etc. Local area networks constituted of this readily available infrastructure can be a cost-effective solution to meet the last mile and last inch challenges of communication. The available PLC system operates in two ranges of frequencies: narrowband PLC (NBPLC) and broadband PLC (BPLC). NBPLC uses the 3–148.5 kHz band governed by CENELAC EN50065 standards in Europe and up to ∼500 kHz by FCC and ARIB in USA and Asia, respectively, catering to low data rate requirements.[1] BPLC uses the (1, 30) MHz band to achieve higher data rates.

As any other communication devices, PLC modems need to be optimized in efficient channel simulators or emulators before deployment. These must be able to replicate the channel as close to reality otherwise would adversely affect the performance of systems in the field. This requires extensive study and modeling of the PL characterized by time, frequency and position dependencies and considered a "horrible"[4] channel for communication. The channel often shows "contradictory" results[5] and cannot be represented by models common to other wired or wireless counterparts. The unambiguous nature of the PL, however, undermines all and motivates modeling of the channel that incorporates every finer details of interest.

A distinctive feature of the PL channel is the noise known to be nonadditive white Gaussian noise (AWGN).[6] Zimmermann and Dostert[6] classified this as a summation of five components depending on their origin, intensity and duration of occurrences; namely colored background noise (CBGN), narrow-band interference (NBI) and three classes of impulsive noise. The CBGN is the part that is always present and varies slowly, remaining constant for minutes and hours caused by summing noises due to many sources, and has a low power spectral density (PSD). The NBIs caused by radio transmitters are also termed as the "narrow-band disturbers" and together with the CBGN constitute the total background noise. The impulsive noises increase the noise levels to much higher levels and are usually of three types: periodic and synchronous or asynchronous with the mains cycle and nonperiodic sporadic (random) in nature. The noise is dependent on the venue and time[7–10] that makes it difficult to be fitted by generalized models. Simulation of noise should take into account the salient features of each of the components to present a realistic environment wherein devices can be optimized for achieving performance even while in the field.

Many methods are used to capture the features of PL noise to regenerate when required. In general, the modeling approach can be divided into two domains: time-domain and frequency-domain approaches.[11] The frequency-domain approach is used for the CBGN and both approaches in the analysis of impulsive noise. Some of the methods are the Middleton's model,[12,13] noisy load affected by the frequency response of the channel,[11,14,15] Markov models for correlating the time variance with loads,[15] filtering white noise through linear filters with predetermined constant multipliers[16] and lastly the Zimmermann technique.[17,18] In the first method, the total noise is categorized by background and impulsive noises depicted by the impulse indexes A and the background-to-impulsive power ratio Γ. As the method was originally developed to model man-made interferences, it is still inconclusive whether the same can be applied to PL impulses.[13] The second and the third methods require knowledge of the channel to be known *a priori*[13–15] which is a practical impossibility. The fourth one needs knowledge of large numbers of multipliers. The Zimmermann technique involves adding the individual components of noise constituting it by empirical models. Accordingly, the mean PSD of CBGN is modeled using a function that decreases with frequency,[17] the impulsive noise by random numbers to select the inter-arrival time and the impulse length following a known statistic,[17] the NBI uses distribution functions for different parameters[18] and the synchronous noise by the cyclo-stationary noise model.[19,20] The advantage of this technique is that every component of noise can be modeled carefully to create a practical channel environment. The success, however, lies in the in-depth analysis of every component, and representation by accurate models.

Though much work has been done on other types of noise, the study, modeling and simulation of the CBGN are neglected and most works are satisfied with the static models (AWGN or time-invariant colored PSD models).[11,17] Serial numbers (i)–(v) in Table 1 generalize some of the models found in the literature. However, it is known that the PSD is not static and usually varies between the worst- and best-case scenarios. The amplitude distribution (AD) is not Gaussian[8] as assumed by most simulations. The CBGN is also dependent on venues, and a single-frequency model cannot be used around the globe for representation.[7] In Ref. 7, the impact of the models on the channel capacity (CC) has been analyzed for more than 23 different settings or sites reported in the literature. Simulations show that a slight change in the order of few dB can lead to a huge change in CC in tens of Mbps. The error is so huge that in BPL, an AWGN approximation would give a better estimation of the channel performance. A successful simulation should therefore be able to incorporate as much as the observed so that the devices under test are subject to realistic channel environment for optimization. This includes replicating the statistical features like the time-varying PSD with the observed amplitude distribution specific to different sites and venues.[18] Moreover, it should be possible to emulate the simulated noise in hardware so that the implemented devices are optimized in a real channel environment before placing in the field. However, an extensive literature review shows that

no such testbeds are available till date and very less work has been done on hardware emulators of CBGN. This paper provides a method where the two requirements of obtaining a time-varying PSD with a non-Gaussian probability distribution (PD) mandated by the experimentally observed at any sites are satisfied within a limit of error. The experimentally observed statistics are termed as the *target* PSD with a time-varying feature and *target* PD of the noise samples. The entire work is divided into four parts: experimental, analysis, simulation and testing (Fig. 1). For this, the indoor PL noise in three sites is captured, and modeled to represent the statistical nature. The same is simulated and also emulated using a data acquisition card (DAQ). The efficiency of the method is found out by comparing the CC and bit error rate (BER) of orthogonal frequency-division multiplexing (OFDM) system of channels corrupted by the simulated and experimentally observed noises. Both the NBPLC (FCC band) and BPLC bands are considered for analysis, referred to here as the low-frequency band (LFB) and

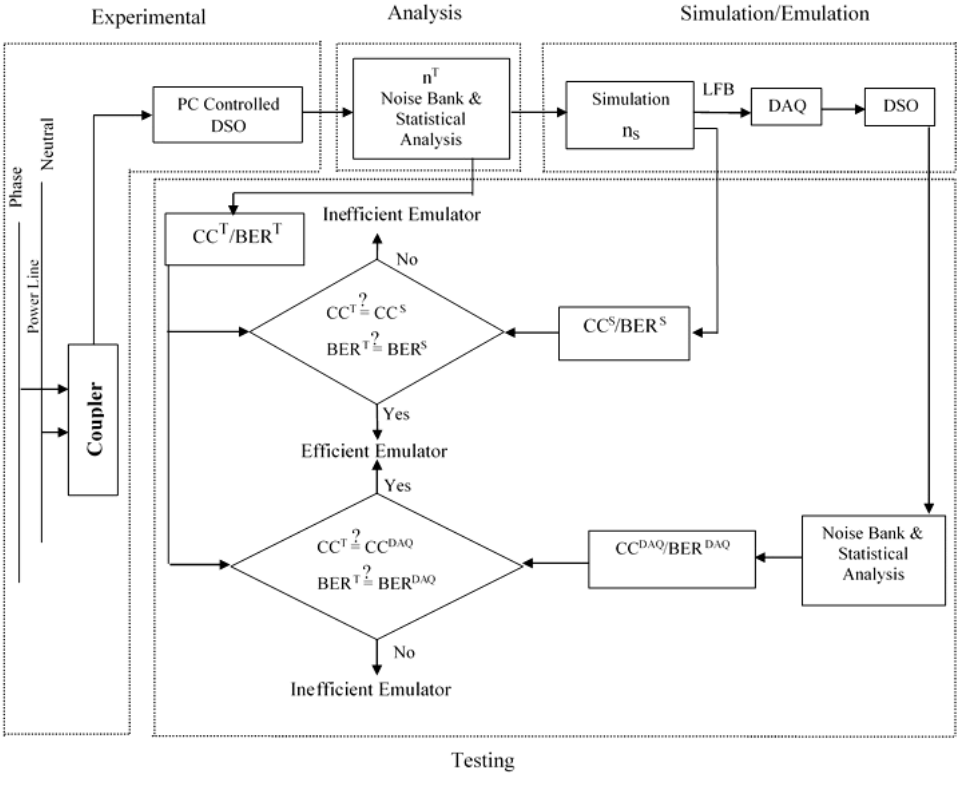

Fig. 1. The block diagram of the methodology used. Here, n^T = captured noise, n_s = simulated noise, DSO = digital storage oscilloscope, DAQ = data acquisition card, LFB = low-frequency band, CC = channel capacity and BER = bit error rate of OFDMA; subscripts E = experimental noise, S = simulated noise and DAQ = noise from data acquisition card.

high-frequency band (HFB), respectively. This method can be incorporated for site-specific CBGN regeneration using Zimmermann technique to get a more realistic channel for system testing and optimization.

The paper is organized as follows: Section 2 gives a literature review of the available schemes for the CBGN modeling and simulation. Section 3 gives the theoretical methods and tools used for the simulation. Section 4 describes the experimental arrangement for the noise data acquisition and analysis. In Sec. 5, the results are used to simulate noise having the target statistics and the efficiency is estimated. This is followed by a discussion on the results in Sec. 6 and the conclusion of the work in Sec. 7.

2. Literature Review of CBGN Models and Simulation Techniques

Modeling and simulation methodologies opted for the CBGN vary. A comparison of available techniques and hardware emulation is tabulated in serial numbers (i)–(xii) of Table 1.

2.1. *Frequency-domain models of the CBGN*

The PSD of CBGN decreases with frequency and can be modeled empirically using suitable fits. Serial numbers (i)–(v) in Table 1 give some of the models found in the literature. The model in (i) summarizes the findings of a number of papers where N_{NF} is the spectral flat AWGN/PSD, and n_1 and n_2 are the coefficients having different values in different observation sites. In (ii), a similar model is obtained after eliminating the NBIs. Here, N_0 is the constant noise power density and N_1 and f_1 are the parameters of the exponential function. In (iii), a, b and c are constants depending on the location of measurement. According to (iv), the noise can be modeled as a function of four parameters a, b, c and d. In (v), this has been applied to LFB and HFB as well. Both the lower- and higher-frequency regions of the band of interest decrease with frequency as reflected in the constants (a, b) and (c, d), respectively. In these models, the PSD varies between the best and worst cases which give the lower and upper bounds of CC. Except in (ii) and (v), the time variations have been neglected providing an incomplete representation of the actual noise scenario.

2.2. *Simulation techniques of CBGN*

Simulation of CBGN is usually based on regenerating noise with the required PSD. Depending on the methodology opted, these are broadly divided here into two categories: the statistical analysis method (SAM) and the spectrum fitting method (SFM). SAM takes into account the statistical fluctuations at every frequency of the PSD and SFM generates noise with the required PSD. Hardware emulators are also opted to regenerate the noise.

Table 1. The salient features of the modeling (empirical) and simulation techniques for colored background noise.

			Modeling features				Simulation features				
No.	Ref.	Bandwidth	Model variable	Model	Frequency (f)	Time variation	Technique	Target PSD	Target PD	Time variation	Remarks
(i)	7	3–30 MHz 3–88 MHz	Noise PSD Noise PSD	$N(f)=N_{NF}+n_1e^{-n_2f}$ (dBm/Hz)	MHz	×	SFM	S	×	×	FFC can be used; varying PSD and target PD cannot be obtained
(ii)	18	3–30 MHz	Noise PSD	$S_{nn}^{(h)}(f)=N_0+N_1\cdot e^{-\frac{f}{f_1}}$ (dBm/Hz)	MHz	√	SFM	S	×	×	Simulation of time-variant noise not done
(iii)	8	<30 MHz	Noise PSD Noise PD	$N(f)=a+b\|f\|^c$ (dBm/Hz) Non Gaussian	MHz	×	SFM	S	×	×	FFC can be used; varying PSD and target PD cannot be obtained
(iv)	9	<60 MHz	Noise PD	$N(f)=ae^{bf}+ce^{df}$ (dB/Hz)	Hz	×	SFM	S	×	×	FFC can be used; varying PSD and target PD cannot be obtained
(v)	10	<500 kHz <30 MHz	Noise PD Noise PD	$N(f)=ae^{bf}+ce^{df}$ (dB/Hz) $N(f)=ae^{bf}+ce^{df}$ (dB/Hz)	Hz Hz	√	SFM	S	×	×	Simulation of time-variant noise not done
(vi)	9	<60 MHz	PDF of NDS at every frequency interval	Nakagami-m Rician		√	SAM	V	×	√	A number of parameters at every frequency interval need to be stored for regeneration, target PD of noise voltage not analyzed
(vii)	11	1–30 MHz	PDF of NDS at every frequency interval	Nakagami-m, Gaussian		√	SAM	V	×	√	A number of parameters at every frequency interval need to be stored for regeneration, target PD of noise voltage not analyzed

Table 1. (*Continued*)

			Modeling features				Simulation features				
No.	Ref.	Bandwidth	Model variable	Model	Frequency (f)	Time variation	Technique	Target PSD	Target PD	Time variation	Remarks
(viii)	21	1–30 MHz	PDF of NDS at every frequency interval	No specific		√	SAM	V	×	√	A number of parameters at every frequency interval need to be stored for regeneration, target PD of noise voltage not analyzed
(ix)	18	1–30 MHz	PDF of NDS at every frequency interval	Gaussian		√	SAM	V	×	√	A number of parameters at every frequency interval need to be stored for regeneration, target PD of noise voltage not analyzed
(x)	22	20–150 kHz	PDF of NDS at every frequency interval	Sum of two Rayleigh distributions		√	SAM	V	×	√	A number of parameters at every frequency interval need to be stored for regeneration, target PD of noise voltage not analyzed
(xi)	23	>1 MHz	PDF of NDS at every frequency interval	Log-normal		√	SAM	V	×	√	A number of parameters at every frequency interval need to be stored for regeneration, target PD of noise voltage not analyzed
(xii)	27	1–50 MHz	Low-pass filter	Direct-type structure		×	SFM	S	×	×	FPGA used
(xiii)	M2	LFB < 0.5 MHz HFB: 1–30 MHz	Noise PSD	$\tilde{S}_M^{n2} = a_r e^{brf} + ce^{drf}$(dB/Hz)	Hz	√	VFC	V	×	√	14 parameters for attaining target time-varying PSD

Table 1. (*Continued*)

			Modeling features				Simulation features				
No.	Ref.	Bandwidth	Model variable	Model	Frequency (f)	Time variation	Technique	Target PSD	Target PD	Time variation	Remarks
(xiv)	M3	LFB < 0.5 MHz HFB: 1–30 MHz	Noise PSD/PD	$\tilde{S}_M^{n2} = a_r e^{brf} + ce^{drf}$ (dB/Hz)/TLS	Hz	√	VFC-PD	V	√	√	17 parameters for attaining time-varying PSD and target PD
(xv)	$M2_{DAQ}$	LFB < 0.5 MHz	Noise PSD	$\tilde{S}_M^{n2} = a_r e^{brf} + ce^{drf}$ (dB/Hz)	Hz	√	VFC	V	×	√	14 parameters for attaining target time-varying PSD
(xvi)	$M3_{DAQ}$	LFB < 0.5 MHz	Noise PSD/PD	$\tilde{S}_M^{n2} = a_r e^{brf} + ce^{drf}$ (dB/Hz)/TLS	Hz	√	VFC-PD	V	√	√	17 parameters for attaining target time-varying PSD and target PD

Notes: PSD: Power spectral density, PD: probability distribution, PDF: probability distribution function, TLS: t-location scale, NDS: noise density spectrum, S: static, V: varying, ×: not applicable and √: Applicable.

2.2.1. *The statistical analysis method*

In this method, the statistical characteristics of the target PSD are captured by calculating the noise density spectrum (NDS) at every frequency interval using a suitable probability distribution function (PDF).[9,11,21–23] Serial numbers (vi)–(xi) in Table 1 give such an analysis. Some PDFs are Gaussian, Nakagami-m, Rician, "sum of two Rayleigh distributions", log-normal, etc. In the backward simulation, random numbers at every frequency interval are generated to synthesize back the net noise voltages.[9] It has been found for Nakagami-m model[11] that multicarrier modulation scheme like OFDM is independent of the type of PDF at each frequency and shows the same results as those in AWGN. But single-carrier modulations like FSK and PSK degrade for these type of channel noise, especially $m < 1$. This is because of the fast Fourier transform (FFT) operation at the OFDM receiver that randomizes the PL noise resulting in Gaussian axis PDF or the PDF of the noise in the real and imaginary axes.[11]

The SAM is able to model and replicate the time-varying nature of the observed noise and the PD of NDS at every frequency. However, the disadvantage of this method is that a number of parameters at every frequency interval are needed to be stored for regeneration. Also, it has not been analyzed if the requirement of the target PD of the noise voltage is obtained.

2.2.2. *The spectrum fitting method*

In this method, white noise is passed through a suitable filter, the transfer function of which is calculated from the trend of the average PSD of the captured noise[11,24] or with the best- and worst-case scenarios.[17] The frequency-domain models given in serial numbers (i)–(vi) of Table 1 can be used as filters for SFM simulations. This method is capable of generating noise with a required PSD which is static in form and the time variation is neglected. Though (ii) and (v) have captured the variation in terms of the distribution fits of the parameters, this has not been utilized to simulate the noise.

The SFM is comparatively simpler than the SAM, but has two major drawbacks. First, the generated noise does not take into account the variation of the target PSD, and so is the conventional method. As the parameters of the filter are always fixed, this can be termed as the *fixed filter configuration* (FFC) method. However, it has been noted earlier that a slight change of the PSD in the order of few dB can lead to a huge change in the CC of tens of Mbps.[7] This requires a method where the variation can be taken into account. Second, the necessity of a target PD of the noise voltages is undermined and the generated noise mostly has a Gaussian or normal probability distribution (NPD). During simulation, even if the noise voltage is initially considered to belong to a target PD, it is no longer so after passing through the filter. As methods to generate noise having a target colored PSD and target PD are lacking, many have settled with AWGN as the CBGN generator.[5,7,25] Gaussian noise on the

other hand has the maximum entropy and gives the worst condition of the channel noise. However, communication systems working in non-Gaussian noise can achieve better performance if designed to adapt to the noise statistics.[26] Adequate methods are therefore required to satisfy the dual requirement simultaneously.

2.3. *Hardware emulators for power line noise*

For a complete simulation package, it is also necessary to develop, test platforms for system testing. A field programmable gate array (FPGA)[27] can be used where the CBGN is produced by passing a pseudo-random sequence through a low-pass filter implemented in a direct-type structure. However, the time variations of the PSD and required target PD are not obtained.

In this paper, two methods are proposed that modify the FFC to incorporate the statistical properties of CBGN with lesser number of parameters. The first is the *varying filter configuration* (VFC), which takes into account the time-varying PSD. The second is the *varying filter configuration with target probability distribution* (VFC-PD) that additionally achieves the target PD. The parameters of the targets are obtained from the analysis of experimental readings. Simulations are also done considering the FFC. The noise generated by the two techniques is also emulated using a DAQ. A comparison of these techniques with earlier works is also shown in Table 1 and remarks the contributions of this paper.

3. Theoretical Basis of Noise Simulation and Emulation

The regeneration of PL noise is based on two mathematical tools namely the inverse cumulative distribution (ICDF) method of generation of random numbers and an iterative method of getting a target PSD of noise samples from a target PD.

3.1. *Random number generation by ICDF function*

The ICDF method is also termed as the inverse transform sampling and is the basic technique for generation of random numbers from any PD. In this method, if u is a uniform random number in the range [0, 1], then the ICDF of the required distribution applied to u will give the random numbers v, having the expected distribution. Thus, if F is the cumulative distribution function (CDF) of the required distribution, then $v = F^{-1}(u)$ generates the necessary samples satisfying this.

3.2. *Iterative technique for getting a target PD with a target PSD*

This technique operates on a Gaussian simulation having the desired spectrum with a nonlinear static transformation to obtain a target non-Gaussian process.[28,29] The requirement of simultaneous satisfaction of a target PSD and a

target PD is obtained by sufficient iterations that update the design spectrum used to create the Gaussian process.

To obtain this, first of all, a Gaussian signal X is generated based on the initial design spectrum $S^D(1)$. This spectrum is also the target spectrum S^T sought for. Thus, in the first iteration $i = 1$ and $S^D(i) = S^T$. X has the required spectrum, but not the target PD. This is now transformed to another signal Y with the desired PD by a nonlinear transformation given by (1):

$$Y = F^{-1}(\phi(X)) \,. \tag{1}$$

Here ϕ is a Gaussian CDF and F^{-1} is the ICDF of the desired PD. The resulting Y, however, no longer has the design spectrum. The next step is to iteratively update the design spectrum as follows:

$$S^D(i+1) = \frac{S^D(i)}{S^Y(i)} S^T \,. \tag{2}$$

Here, $S^D(i+1)$ is the new design spectrum and $S^Y(i)$ is the spectrum of Y. The new spectrum is now used to generate the Gaussian process and the iteration is continued till the error between the output spectra and the target is acceptable. The process produces a signal Y that is transformed to a realization of X that has the target spectrum S^T. The exact satisfaction of the targets (both PSD and PD) simultaneously can however be obtained only when the autocorrelations of the Gaussian and non-Gaussian processes span over a similar range. If this is not so, then the transformation cannot produce the target spectrum whatever is the design spectrum.[28,29]

4. Experimental Setup for CBGN Acquisition and Statistical Analysis

The experimental arrangement for acquiring the CBGN and analysis are given in the following.

4.1. *Experimental setup*

The arrangement consists of a PC-controlled digital signal oscilloscope (DSO; Agilent; 1,012 A, 100 MHz, 2 GS/s) connected to the phase–neutral pair of an indoor PL, through a coupler (Fig. 1). The coupler constituted of suitable combinations of 1:1 transformer and capacitors, acts as a passive high-pass filter (cutoff 15 kHz) having a flat frequency response over a broad range of frequencies. The coupler prevents 50 Hz and 230 V of the PL from harming the connected instruments. Data acquisition is done in indoor PLs of three different buildings on the university campus denoted as *Site* 1, *Site* 2 and *Site* 3 for three-week duration at regular intervals. The NBIs are found to be absent in these sites and the effect of the impulse is neglected due to the small probability of occurrences. As such, the total background noise is the CBGN in our case. The noise captured acts as a noise bank n^T for further analysis.

4.2. *Statistical analysis of observed CBGN*

The analysis includes evaluating the amplitude statistics of the noise voltages and the time variation of PSD in terms of suitable distributions. The applicability of the distribution fits for any variables is tested using the Kolmogorov–Smirnov (KS) two-sample goodness-of-fit test with 5% significance level. The KS statistics is the maximum difference between the cumulative distributions of samples from two distributions and is defined by

$$D = \max_X |F_1(x) - F_2(x)|, \tag{3}$$

where $F_1(x)$ and $F_2(x)$ are the observed CDFs of the two samples, respectively, and the maximization is with respect to x. If D is less than the critical value of the samples, then the null hypothesis that the samples are from the same distribution is accepted, otherwise rejected. The value of the statistics gives the deviation from the null hypothesis. If the variable does not comply strictly with a known distribution, then that with the lowest statistics is taken. The distributions tested are the normal, t-location scale (TLS), logistic, Nakagami-m, Rayleigh, Rician, etc.

4.2.1. *The PD of the noise amplitude*

In all the sites and bands, the AD of the noise voltages shows non-Gaussian distributions namely the TLS distribution.[30] Table 2 gives the parameters of the TLS distribution for all the sites and bands. Figure 2(a) gives an example of the distribution for *Site* 1 in the HFB. The TLS distribution function is given by[30]

$$f(x) = \frac{\Gamma\left(\frac{\nu+1}{2}\right)}{\sigma\sqrt{\nu\pi}\,\Gamma\left(\frac{\nu}{2}\right)}\left[\frac{\nu + \frac{x-\mu}{\sigma}}{\upsilon}\right]^{-\left(\frac{\nu+1}{2}\right)}, \tag{4}$$

where Γ is the gamma function, μ is the location parameter, $\sigma$is the scale parameter and $\nu$is the space parameter. The scale parameter gives a measurement of the statistical dispersion of PD. The TLS distribution has heavier tails than the Gaussian distribution. Superposition of NPD with the same mean and standard deviation in the figure shows the unsuitability of being represented by this function.

4.2.2. *Frequency-domain modeling and statistical analysis of the model parameters*

As the NBIs were found to be absent, the PSD of the noise samples after smoothing with a moving average filter enabled the empirical model to be obtained. Figure 2(b) shows the PSD in *Site* 1 in the HFB. In all the sites, the PSD decreases with frequency and follows a four-parameter (*a, b, c, d*) model given by (v) in Table 1. The PSD varies between considerable limits in all the sites, and the best- and worst-case parameters are given in Table 3.

To perform a statistical analysis of the variations, the parameters a, b, c and d are fitted with suitable distributions, the parameters of which are given in Table 2. The

Table 2. The parameters of the probability distribution functions for different fits.

Low-frequency band (<500 kHz)						
	Site 1		*Site* 2		*Site* 3	
	PDF	Parameters	PDF	Parameters	PDF	Parameters
AD	TLS	$\mu = 0.026$, $\sigma = 0.035$, $\nu = 3.743$	TLS	$\mu = 0.067$, $\sigma = 0.34$, $\nu = 6.59$	TLS	$\mu = 0.054$, $\sigma = 0.2$, $\nu = 2.323$
a	TLS	$\mu = -105.05$, $\sigma = 2.56$, $\nu = 1.47$	TLS	$\mu = -96.73$, $\sigma = 4.04$, $\nu = 2.30$	TLS	$\mu = 0.78$, $\sigma = 0.86$, $\nu = 0.59$
b	NA	—	—		NPD	$\mu = 2.11 \times 10^{-6}$, $\sigma = 1.01 \times 10^{-6}$
c	TLS	$\mu = 39.57$, $\sigma = 4.18$, $\nu = 2.37$	TLS	$\mu = -37.05$, $\sigma = 3.77$, $\nu = 1.81$	NA	—
d	NPD	$\mu = -1.47 \times 10^{-5}$, $\sigma = 7.8 \times 10^{-6}$	NPD	$\mu = -1.43 \times 10^{-5}$, $\sigma = 8.03 \times 10^{-6}$	NPD	$\mu = 3.37 \times 10^{-7}$, $\sigma = 1.45 \times 10^{-7}$
High frequency band (1–30 MHz)						
	Site 1		*Site* 2		*Site* 3	
AD	TLS	$\mu = 0.009$, $\sigma = 0.002$, $\nu = 3.743$	TLS	$\mu = 0.048$, $\sigma = 0.189$, $\nu = 2.99$	TLS	$\mu = 0.19$, $\sigma = 0.03$, $\nu = 2.66$
a	TLS	$\mu = -144.45$, $\sigma = 2.5$, $\nu = 2.35$	TLS	$\mu = -126.61$, $\sigma = 3.48$, $\nu = 1.71$	TLS	$\mu = -124.34$, $\sigma = 3.98$, $\nu = 3.95$
b	NA	—	NA	—	TLS	$\mu = 9.566 \times 10^{-11}$, $\sigma = 1.56 \times 10^{-10}$, $\nu = 8.26$
c	TLS	$\mu = 25.56$, $\sigma = 3.74$, $\nu = 6.4$	TLS	$\mu = 28.85$, $\sigma = 7.3$, $\nu = 4.28$	TLS	$\mu = 27.75$, $\sigma = 8.11$, $\nu = 1.54$
d	NPD	$\mu = -4.19 \times 10^{-8}$, $\sigma = 1.78 \times 10^{-8}$	NPD	$\mu = -6.05 \times 10^{-8}$, $\sigma = 4.087 \times 10^{-8}$	NPD	$\mu = -5.90 \times 10^{-8}$, $\sigma = 3.18 \times 10^{-8}$

Notes: PDF: Probability distribution function, AD: amplitude distribution, TLS: t-location scale, NPD: normal probability distribution and NA: no distribution available.

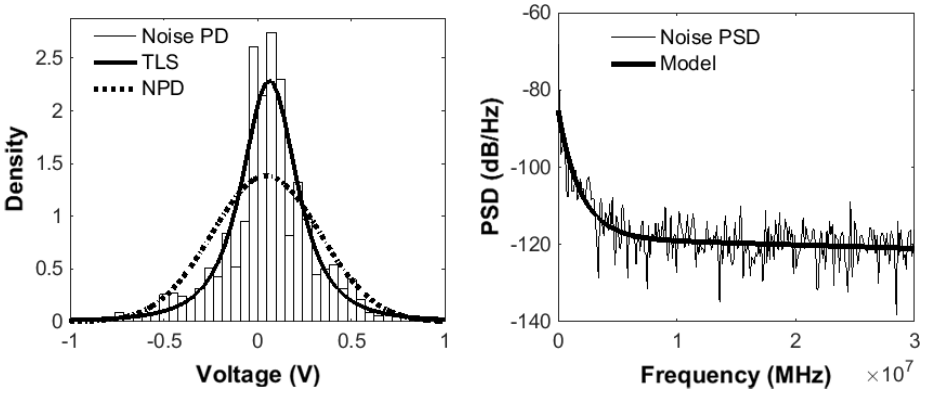

(a) (b)

Fig. 2. (a) The PD of the noise voltage in *Site* 1 (HFB) showing the TLS distribution and NPD fit. (b) The PSD of the noise in *Site* 1 (HFB).

distributions for *Site* 1 in the LFB are shown in Fig. 3. It is seen from the table that the parameters a and c satisfy the TLS distribution for all the cases, except in the LFB of *Site* 3. However, d follows the NPD for all the sites. The distribution of b cannot be generalized for *Site* 1 and *Site* 2 but follows the NPD and TLS in LFB and HFB, respectively, in *Site* 3. The interdependence of the parameters in each site is found out using the correlation coefficient (ρ), the values of which are given in Table 4. Figure 4 shows the scatter-plots of a–b, a–c and a–d noting the correlation coefficient ρ in the LFB of *Site* 1. As shown in the table, the parameters (a, b) have high correlation in *Site* 1 and *Site* 2 in both the bands, whereas the parameters (a, c) have a high negative correlation only in the LFB of *Site* 3. The parameters (a, d) have low correlation in all the sites and bands. None of the parameters in the HFB of *Site* 3

Table 3. Best- and worst-case model parameters of the power spectral density in different sites and bands.

Site	Band	Case	a	b	c	d
Site 1	LFB	Best	-125.48	-1.66×10^{-8}	50.98	-3.25×10^{-5}
		Worst	-100.01	4.77×10^{-8}	37.84	-1.35×10^{-5}
	HFB	Best	-136.22	3.42×10^{-10}	28.64	-3.77×10^{-7}
		Worst	-136.60	-6.3×10^{-11}	32.80	-3.2×10^{-7}
Site 2	LFB	Best	-96.08	5.42×10^{-8}	36.20	-2.3×10^{-5}
		Worst	-90.43	7.6×10^{-8}	36.49	-1.8×10^{-5}
	HFB	Best	-124.80	2.07×10^{-10}	37.03	-1.1×10^{-7}
		Worst	-119.33	1.97×10^{-10}	27.30	-5.7×10^{-8}
Site 3	LFB	Best	0.367	2.55×10^{-6}	-89.42	1.35×10^{-7}
		Worst	0.638	2.23×10^{-6}	-68.03	2.87×10^{-7}
	HFB	Best	0.815	1.11×10^{-8}	-118.25	5.07×10^{-10}
		Worst	-198.21	-1.2×10^{-9}	91.19	-6.40×10^{-9}

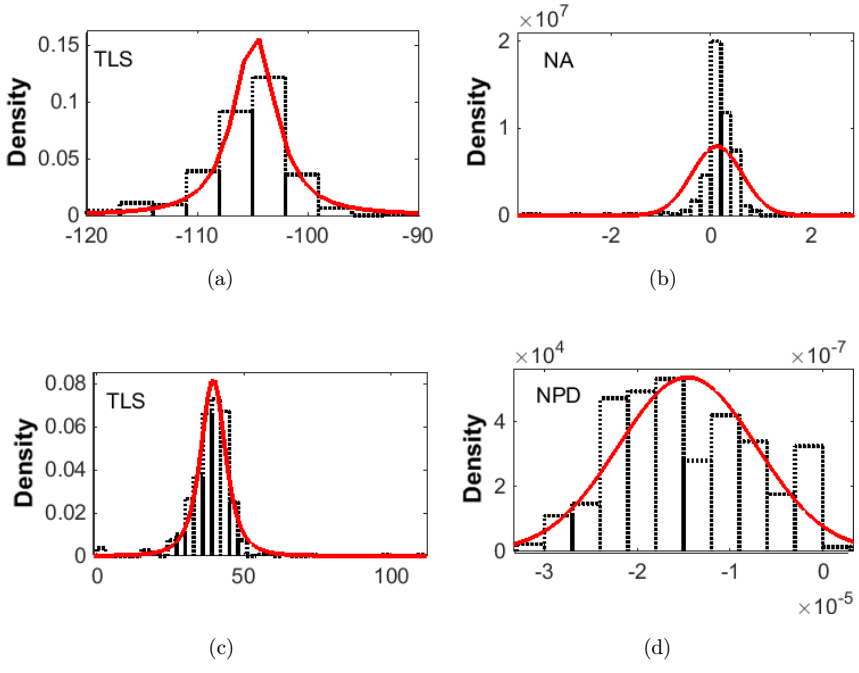

Fig. 3. The probability densities of the modeling parameters in the LFB in *Site* 1. TLS: t-location scale, NPD: normal probability distribution and NA: no distribution available.

showed a correlation greater than 0.7. The parameters whose correlations are high ($|\rho| > 0.8$) can be modeled using a linear fit specified by (M, C) as shown below:

$$y_{b/c} = Mx_a + C\,. \tag{5}$$

The values of (M, C) are given in Table 4. Here the independent (x) and dependent parameters (y) are a and b/c, respectively. As seen from the table, the R^2 value of the linear fit is found to be high. The parameters of *Site* 3 in the HFB could not be fitted

Table 4. The correlation coefficients and straight line fits of correlated parameters.

Parameter/Band		LFB	LFB	LFB	HFB	HFB	HFB
		Site 1	*Site* 2	*Site* 3	*Site* 1	*Site* 2	*Site* 3
ρ	a–b	0.8	0.87	−0.24	0.96	0.85	0.77
	a–c	−0.4	−0.35	−0.95	−0.23	−0.14	−0.017
	a–d	−0.4	−0.28	0.22	−0.7	0.33	−0.53
	(x, y)	(a, b)	(a, b)	(a, c)	(a, b)	(a, b)	NA
St.	M	7.34×10^{-9}	8.92×10^{-9}	−1.118	3.0×10^{-11}	3.0×10^{-11}	NA
line	C	7.81×10^{-7}	8.87×10^{-7}	−75.36	4.0×10^{-9}	4.0×10^{-9}	NA
fit	R^2	0.9	0.9	0.92	0.938	0.8	NA

Note: The M and C are the straight line fits of (x, y) given in the table for parameters with $|\rho| > 0.8$. NA: Not available.

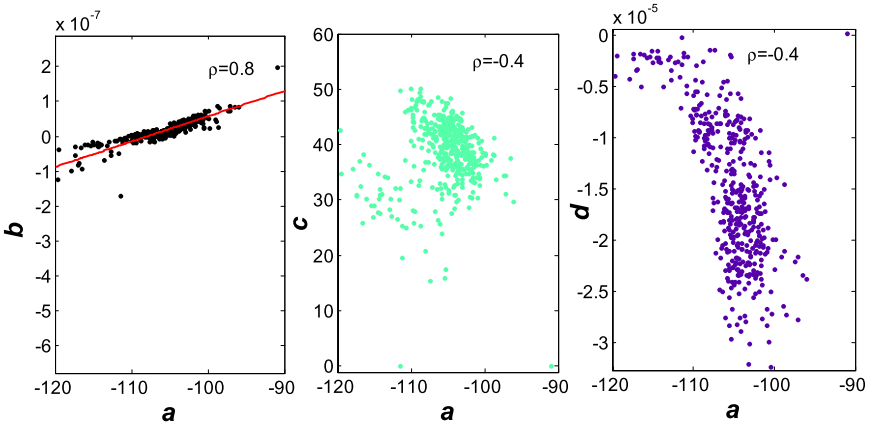

Fig. 4. The scatter-plots of a–b, a–c and a–d showing the correlation coefficients ρ in the LFB of *Site* 1.

by linear models and denoted by "NA" in the table. The obtained parameters are used to simulate the CBGN in the next section.

5. Simulation of CBGN and Testing

This section aims to generate noise specific to the sites that efficiently follow the statistics both in the frequency and amplitude domains represented by Table 2. The efficiency of the simulation methodologies is also evaluated thereafter.

5.1. *Simulation of CBGN*

The ultimate aim of the simulation is to attain two objectives. First, the target PSD is that whose model follows the statistics of the parameters (a, b, c, d). The target model sought for is denoted by $\tilde{S}_M^T(f)$. The symbol "$\sim$" categorizes it as having a time-varying nature, subscript M represents the model and the superscript T depicts that it is the target model aimed for. Second, the target PD of the noise voltages is the TLS distribution with the observed values of the parameters and is denoted by n_{PD}^T. Three methods are used: Method 1 (M1), Method 2 (M2) and Method 3 (M3). Method 1 is the conventional or FFC used as a basis for further simulation. Method 2 and Method 3 are the VFC and the VFC-PD, respectively. The flowcharts of all the three methods are shown in Fig. 5. The output of the simulation using the three methods is represented by $n_s(t)$ which can be $n_1(t)$, $n_2(t)$ or $n_3(t)$ with PDs denoted by $n_{1\mathrm{PD}}$, $n_{2\mathrm{PD}}$ and $n_{3\mathrm{PD}}$, respectively.

5.1.1. *Method* 1 (*conventional*): *CBGN having average PSD* (*FFC*)

This is the conventional method commonly used for noise simulation with a required PSD in the SFM. For this, the average of all the observed PSDs is taken, and a filter

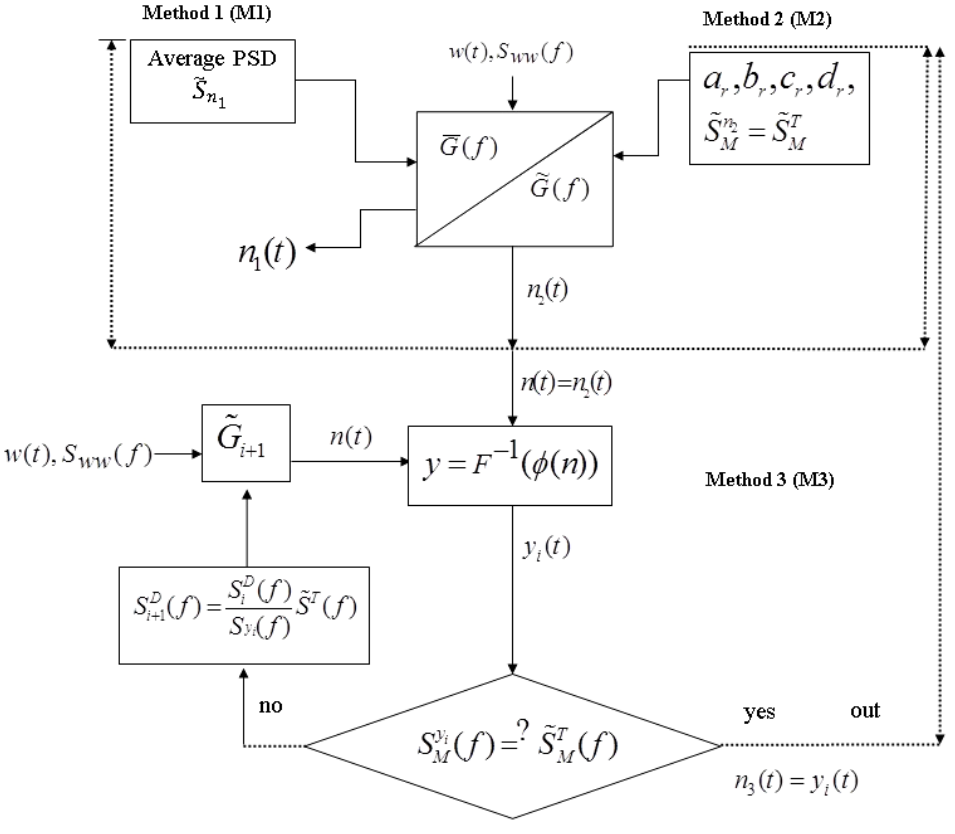

Fig. 5. The block diagram of the different simulation methods.

having a corresponding response is designed. The finite impulse response (FIR) filter uses the frequency sampling technique[31] by which any arbitrary magnitude response can be achieved. White noise passes through this filter, thereby generating noise having the average PSD.[18]

In Fig. 5, $w(t)$ and $n_1(t)$ are the input and generated noise having PSDs $S_{ww}(f)$ and $\bar{S}_{n1}(f)$, respectively. (f) is the frequency response of the filter. The superscript "–" categorizes it as having a time-invariant nature. $S_{ww}(f)$ is given by (6) where σ_{ww} is the variance:

$$S_{ww}(f) = \sigma_{ww}^2 . \tag{6}$$

$\bar{S}_{n1}(f)$ is the time average or the expectation (ε) of the measured PSD represented by $S_{nn}^{\text{meas}}(f,t)$, and is given by

$$\bar{S}_{n1}(f) = \varepsilon\{S_{nn}^{\text{meas}}(f,t)\}_t . \tag{7}$$

The response of the filter to obtain this[18] is given by

$$(f) = \sqrt{\frac{\bar{S}_{n1}(f)}{S_{ww}(f)}} = \frac{\sqrt{\bar{S}_{n1}}}{\sigma_{ww}} \,. \tag{8}$$

As noted earlier, the limitations of this method are that the same PSD is generated every time, and does not represent the time-variant CBGN truly. The model of PSD of the output noise denoted by $\bar{S}_M^{n1}(f)$ is not what is desired and the target PD is also not obtained. The following results are concluded:

$$\bar{S}_M^{n1}(f) \neq \tilde{S}_M^T(f) \,, \tag{9}$$

$$n_{1\mathrm{PD}} \neq n_{\mathrm{PD}}^T \,. \tag{10}$$

The method is therefore an inefficient emulator of the statistics of CBGN.

5.1.2. *Method* 2: *CBGN having the statistics of the target PSD* (*VFC*)

In M2 the model fit of the PSD of the generated noise has the statistical nature of $\tilde{S}_M^T(f)$. To achieve this, the model parameters are obtained randomly. In every simulation of noise samples, four random numbers a_r, b_r, c_r and d_r corresponding to the parameters a, b, c and d, respectively, and having the desired statistics are generated (Fig. 5). Two techniques are used for generation. The first is for the parameters that can be represented by suitable PD as given in Table 2 and the second is for those which cannot be fitted adequately but are correlated to the first type as given in Table 4. For the former, the random numbers are directly generated, using the ICDF technique discussed in Sec. 3.1. For the latter, the independent parameters which can be fitted by distribution fits are at first generated. The dependent one is then evaluated using the linear fit equation (5). In all the generations, the parameter a is the independent variable that can be suitably fitted by TLS distribution in all the sites and bands and the dependent variable is b/c as shown by Table 4. The desired PSD of the output noise $n_2(t)$ is then expected to be fitted by the model (11).

$$\tilde{S}_M^{n2}(f) = a_r e^{b_r f} + c_r e^{d_r f} (\mathrm{dB/Hz}) \,. \tag{11}$$

A filter is then designed which manipulates an input white Gaussian noise $w(t)$ to give $n_2(t)$. The transfer function of the filter is given by (12):

$$\tilde{G}(f) = \frac{\sqrt{\tilde{S}_M^{n2}}}{\sigma_{ww}} = \frac{\sqrt{a_r e^{b_r f} + c_r e^{d_r f}}}{\sigma_{ww}} \,. \tag{12}$$

At every generation of the noise samples, a new filter is generated using the random numbers, and the model fit of the PSD of the resultant follows the statistics of the

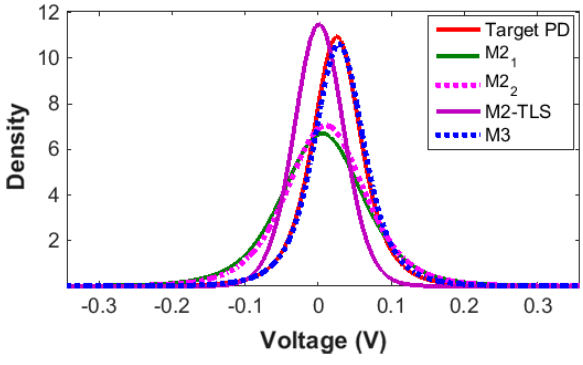

Fig. 6. The PD of the simulated noise in *Site* 2 (LFB) when the input has a Gaussian distribution ($M2_1$ and $M2_2$) and a TLS distribution (M2-TLS) compared against the experimentally obtained one (target PD). M3 represents the distribution obtained using Method 3.

target $\tilde{S}^T_M(f)$. This is because, every time generated, the parameters a_r, b_r, c_r and d_r are samples from the observed PDFs.

In this method, though the requirement of the target PSD with a varying feature is obtained, the output noise voltages do not have the distribution of the target PD. This is the case even when the input noise is considered to satisfy the required PD initially. Figure 6 shows the distribution of the output when the input has a Gaussian distribution ($M2_1$ and $M2_2$) and a TLS distribution (M2-TLS). For convenience, the PD of the TLS distribution or the target distribution is also plotted in the same figure. In none of the cases the target PD is achieved. This method therefore generates

$$\tilde{S}^{n2}_M(f) = \tilde{S}^T_M(f)\,, \tag{13}$$

$$n_{\text{2PD}} \neq n^T_{\text{PD}}\,. \tag{14}$$

The limitation of this method is met in M3.

5.1.3. *Method* 3: *CBGN having the statistics of the target PSD and target PD (VFC-PD)*

The aim in M3 is to generate noise following the statistics of $\tilde{S}^T_M(f)$ with a target PD every time generated. The block diagram of the method is shown in Fig. 5. For this, the iterative technique described in Sec. 3.2 is used. To apply this, the PSD of noise generated by M2 is taken as the target PSD or design spectrum and is denoted by $\tilde{S}^T(f)$. The "$\sim$" symbol represents the time-varying nature and follows the statistics of the observed when simulated every time. It is now required to generate a non-Gaussian noise for every simulated target through a number of iterations. In the first iteration, the target PSD is taken as the initial design spectrum $[S^D_1(f) = \tilde{S}^T(f)]$ and

a Gaussian signal having this spectrum is obtained. Non-Gaussian signals y_1 having a TLS distribution with the required parameters are then generated through a non-linear transformation (1). In order to check the nature of the PSD of y_1, the model fit is compared with that of $n_2(t)$. The model fits are given by $S_M^{y_i}(f)$ and $S_M^{n_2}(f)$, respectively, in the figure. If there is a deviation of more than 5 dB/Hz at any frequency and the models have a correlation lesser than 0.8, then the design spectrum is updated in accordance with (2) using (15):

$$S_2^D(f) = \frac{S_1^D(f)}{S_{y_1}(f)} \tilde{S}^T(f)\,. \tag{15}$$

Here, $S_{y_1}(f)$ and $S_2^D(f)$ are the spectra of y_1 and the updated design, respectively. This iteration is continued till the correlation between the models is greater than 0.8 and a maximum deviation at any frequency is less than 5 dB/Hz. If this condition is satisfied, then the simulated noise gives the final output noise voltage or $n_3(t) = y_i(t)$. In general, the design spectrum is updated as

$$S_{i+1}^D(f) = \frac{S_i^D(f)}{S_{y_i}(f)} \tilde{S}^T(f)\,. \tag{16}$$

The transfer function of the filter required to regenerate the Gaussian process is given by $\tilde{G}_{i+1}$. In the next generation of the noise samples, the target spectrum is again updated according to the statistics of a, b, c and d; and the procedure is followed producing a new set of noise samples.

Figure 7 shows an example of the convergence of PSD and PD to the targeted in five iterations. It is seen from the figure that the noise $n(t)$ generated initially does not have the *target* PD but has the *target* PSD (first iteration). After the first iteration, the noise has the target PD, but not the PSD. Similar is the case with the

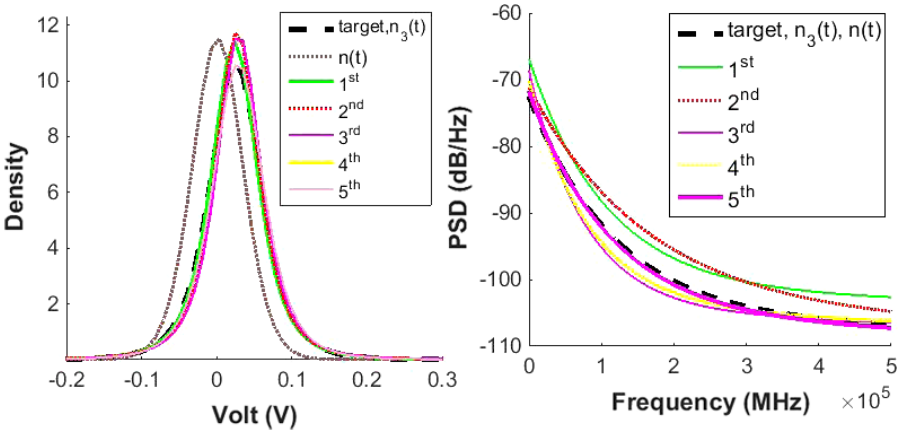

Fig. 7. The PD and the PSD of the target and the output of M3 after each iteration from one to five.

second, third and fourth iterations. In the fifth iteration the PSD and the PD of the generated noise samples converge to the targeted within expectable limits. This is also shown in Fig. 6 where the PD of the noise due to M3 attains the target which was not obtained for M2. The results of this method are

$$\tilde{S}_M^{n3}(f) \cong \tilde{S}_M^T(f)\,, \tag{17}$$

$$n_{3\mathrm{PD}} \cong n_{\mathrm{PD}}^T\,. \tag{18}$$

Here, $\tilde{S}_M^{n3}(f)$ is the model fit of the PSD of the generated noise $n_3(t)$. This method is therefore, an efficient emulator of the statistics of CBGN compared to M1 or M2.

5.2. *Testing the efficiency of the simulation methodologies*

The efficiency of the simulation methodologies is tested in two domains in a time-variant scenario: first, the frequency-domain representation of the statistics and second, the amplitude statistics of the noise samples. For the former, the CC is estimated for channels corrupted by the experimentally obtained and the simulated noises. The percentage errors of the mean and the standard deviation are taken as a measure of the suitability to represent the variant PSD. For the latter, the correlation of the distribution of BER of OFDM at every transmit power in a channel corrupted by the observed and simulated noises (both M2 and M3) is found out. A higher degree of correlation represents a greater capability of attaining the target TLS distribution. The simulated noise is also emulated through the DAQ and the efficiency is estimated. The testing methodology is shown elaborately in Fig. 1. In the figure, CC^T and BER^T are the target features of the CC and BER using the experimentally observed noise, CC^{S} and $\mathrm{BER}^{\mathrm{S}}$ are the features due to the simulated noise and $\mathrm{CC}^{\mathrm{DAQ}}$ and $\mathrm{BER}^{\mathrm{DAQ}}$ using the noise emulated by the DAQ. If the characteristics of CC^{S}, $\mathrm{BER}^{\mathrm{S}}$, $\mathrm{CC}^{\mathrm{DAQ}}$ and $\mathrm{BER}^{\mathrm{DAQ}}$ are comparable to corresponding CC^{T} and $\mathrm{BER}^{\mathrm{T}}$, then the emulation is taken to be efficient otherwise not.

5.2.1. *Estimation of the channel capacity*

The observed noise is non-Gaussian so it is difficult to estimate the CC. However, the Gaussian noise with the same PSD minimizes the capacity, and can be taken as the lowermost limit.[32,33] As such, the capacity is evaluated for the nonwhite PSDs assuming a Gaussian noise using the water-filling approach. This approach is applicable for any channel $H(f)$ acting as a linear filter and corrupted with a Gaussian noise having a PSD of $N(f)$, be it white or nonwhite. For such a channel, the CC is evaluated by summing the capacities of several subchannels which exhibit flat fading characteristics corrupted by the AWGN noise. For such a channel, the CC is given by

$$\mathrm{CC} = \int_{f\in F_B} \frac{1}{2}\log_2\left[\frac{|H(f)|^2 B}{N(f)}\right] df\,, \tag{19}$$

where F_B is the range of frequency where (20) is satisfied:

$$\frac{N(f)}{|H(f)^2|} \leq B\,. \tag{20}$$

And B is a parameter which implicitly depends on the maximum power. Equation (20) signifies that only the frequency band F_B in a colored noise scenario is effective in adding to capacity.[33] To observe the effect of only the variant noise, the channel is considered to be ideal with $|H(f)| = 1$ over the entire bandwidth (BW), and the noise PSD is that given by the model. While evaluating the CC, the model is approximated by two linear fits in the high- and low-frequency regions of the bands. The CC is estimated at the maximum transmit power; considered here to be 0.5 W and 5 μW in the LFB and HFB, respectively. At these transmit powers, the solution can be either of the two cases represented in Fig. 8 shown for the HFB. In the first case, B is much greater than $N(f)$ at all frequencies and as such the entire bandwidth constitutes $F_B = [1, 30]$ MHz and adds to the capacity; however in the second case, only the band $F_B = [f_B, 30]$ MHz achieves the capacity because below f_B, the condition (20) is not met. $S_{\text{rec}}(f)$ is the received power. Figure 9 shows the probability distributions of CC in all the bands and sites. It is seen that the distributions for the simulated (M2 and M3) have close resemblance with those evaluated using the experimental noise. The mean and the standard deviation of CC are provided in Table 5. The percentage errors of these quantities (μ_e% and σ_e%, respectively) in the LFB are found to be as small as 2.17% and 5.26% using M2 and 10.13% and 4.08% using M3. In the HFB, these are found to be 3.03% and 21.18% for M2 and 1.81% and 22.86% for M3. This shows that both two methods represent the statistical variations of the observed PSD within a limit of error. The noise produced by M1, however, produces the same capacity every time simulated due to the static nature of the average PSD.

5.2.2. *Estimation of BER of OFDMA*

The multicarrier modulation, OFDM, is a promising technique for PLC. This modulation has a high spectral efficiency, and can be used to mitigate the harsh

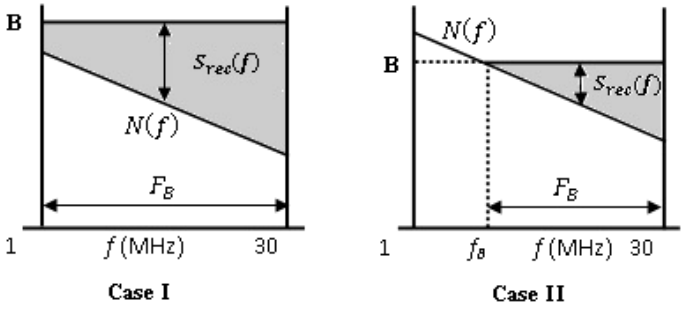

Fig. 8. Interpretations of Case I and Case II of water filling approach.

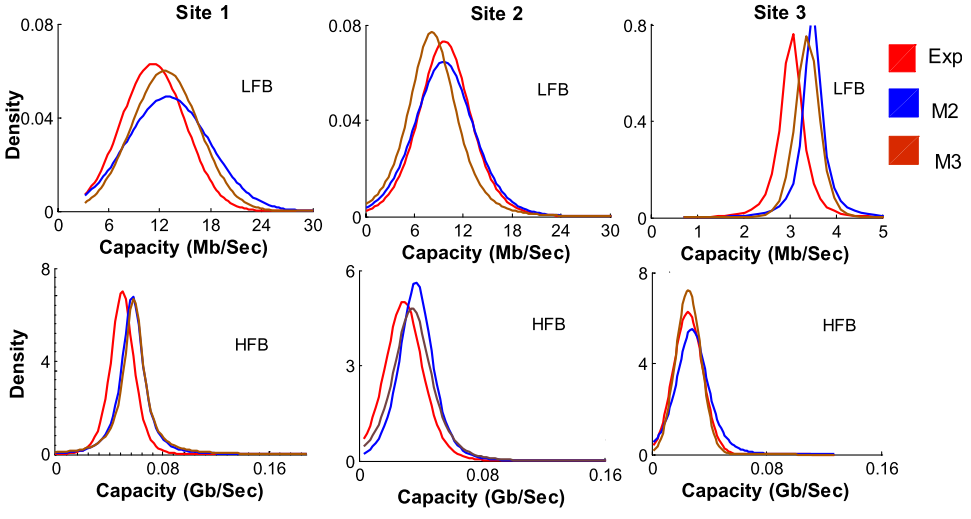

Fig. 9. The probability distributions of the channel capacity in the LFB and HFB in the three sites with experimental and simulated noises using the methods M2 and M3.

effects of multipath propagation, typical to PL channels. Here, the available BW is divided into a number of orthogonal subcarriers, and a high-data-rate bit stream is split into lower ones and sent in parallel through the subcarriers. The property of the subcarriers prevents the bit streams from interfering with each other. If the data BW in each subchannel is less than its coherence one, then inter-symbol interference is removed. In a typical PLC, the received signal is given by

$$r(t) = s(t)h(t) + \tilde{n}(t)\,, \tag{21}$$

where $s(t)$ is the transmitted OFDM signal to the PLC channel, $h(t)$ is the impulse response of the channel and $\tilde{n}(t)$ is the channel noise. The transfer function is the Laplace transform of $h(t)$. Various models are available to model the multipath environment of the PL. However, for simplicity, to observe the effects of noise only, we assume an ideal channel whose transfer function is flat in the entire BW. The PLC system uses a modulation constellation of 16 quadrature amplitude modulation (QAM) OFDM systems. The BER of M-ary QAM OFDM in AWGN is given by (22),[34] but here a nonwhite noise is considered:

$$P_e = \frac{\sqrt{M-1}}{\sqrt{M\log_2\sqrt{M}}}\,\mathrm{erfc}\left(\sqrt{\frac{3.\log_2 M.E_b}{2(M-1).N_0}}\right). \tag{22}$$

In (22) E_b is the energy/bit and N_0 is the noise spectral density. In the simulation, $\tilde{n}(t)$ is time-varying considered to be the experimentally obtained or simulated by the model. At every transmit power (t_0), the OFDM signal thus experiences different

Table 5. The mean and standard deviation values of the channel capacity using the experimental noise, simulated noise and emulated noise using DAQ.

	Site 1				*Site* 2				*Site* 3			
Parameters	μ (Mbps)	σ (Mbps)	μ_e (%)	σ_e (%)	μ (Mbps)	σ (Mbps)	μ_e (%)	σ_e (%)	μ (Mbps)	σ (Mbps)	μ_e (%)	σ_e (%)
Low frequency												
Exp	9.26	3.19			8.29	3.23			2.98	0.48		
M1	10.20	NA	10.15	NA	8.35	NA	7.20	NA	3.52	NA	18.12	NA
M2	10.81	4.07	16.74	27.19	8.11	3.40	2.17	5.26	3.47	0.29	16.44	39.58
M3	10.54	3.32	13.82	4.08	7.45	3.42	10.13	5.88	3.40	0.29	14.09	39.58
$M2_{DAQ}$	10.48	3.18	13.17	0.31	9.02	5.52	13.12	70.87	3.80	0.25	27.51	57.5
$M3_{DAQ}$	10.33	2.98	11.56	6.58	8.04	3.13	3.10	3.10	3.60	0.47	20.80	2.08
High frequency												
Exp	43.90	10.0			46.10	24.90			37.00	10.70		
M1	45.60	NA	3.87	NA	45.10	NA	2.27	NA	35.00	NA	3.90	NA
M2	55.50	17.0	26.42	21.43	44.70	42.50	3.03	21.18	34.20	29.80	7.56	29.29
M3	56.10	17.2	27.79	22.86	47.20	13.83	2.39	38.39	41.00	20.90	1.81	33.12

Note: NA: Not applicable.

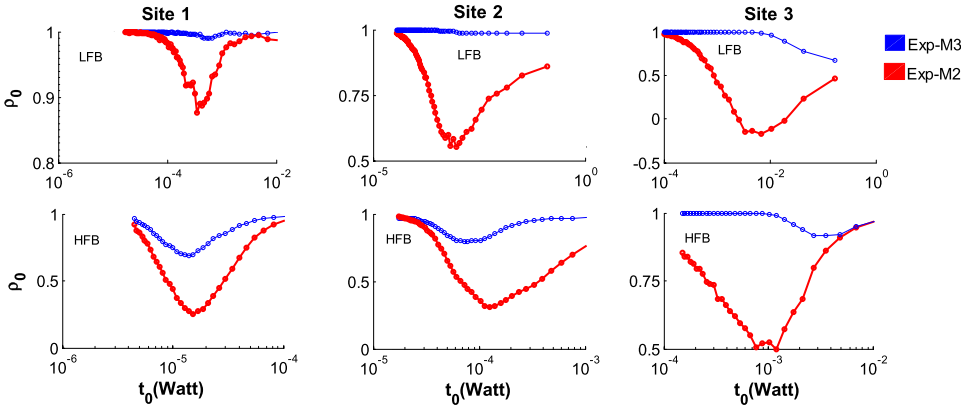

Fig. 10. The plots of (t_0, ρ_0) in the LFB and HFB for all the sites.

channel conditions and the BER changes in accordance to the ratio (E_b/N_0). The distribution of the BER gives a measure of the effect of the variant noise which is modeled using suitable nonparametric distribution fits. The BER is found out for three cases: first with the experimentally obtained noise (Exp), second with the noise generated by M2 and third with the noise generated by M3. The correlation coefficients (ρ_0) for the distributions Exp–M2 and Exp–M3 are then found out. High values of ρ_0 depict that the OFDMA signal in M2 or M3 is affected in a similar way as by the experimental noise. Low values of ρ_0 depict that the signal is affected in a different way. The transmit power t_0 of $s(t)$ is changed at an interval and for each value, the ρ_0 is likewise found out. Figure 10 shows the plots of $(t_0,\ \rho_0)$ for all the bands and sites. Figure 11 shows examples of high and low correlations between the distributions at different values of t_0 namely at extreme $(0.13\,\mathrm{W}/0.03\,\mu\mathrm{W})$ and intermediate $(0.73\,\mathrm{mW}/0.9\,\mathrm{mW})$ values for *Site* 2 (LFB). It is seen from the figures that at $t_0 = 0.13\,\mathrm{W}/0.03\,\mu\mathrm{W}$, the shapes of the three distributions are nearly the same, the which results in high ρ_0 of 0.86/0.99 and 0.98/0.99 in the Exp–M2 and Exp–M3 distributions, respectively. However, for $t_0 = 0.73\,\mathrm{mW}/0.91\,\mathrm{mW}$, the shape of Exp is more similar to that of M3 than M2. This gives ρ_0 of 0.59/0.99 and 0.55/0.99 in the Exp–M2 and Exp–M3 distributions. The reason behind this is that at small values of t_0 all the three cases suffer high BER due to the low value of E_b/N_o and hence result in high values of ρ_0. At very high values of t_0, the BER is always small due to the large ratio. At intermediate power, the distribution of BER in M3 is more like that with the Exp than the M2. This is because the noise generated by M3 follows both the PSD and PD of the experimentally observed due to which the OFDMA signal experiences similar channel conditions as the experimentally observed noise. However, the noise generated by M2 does not attain the target PD and as such the distribution of BER shows low correlation compared to the former. This analysis shows that the BER is sensitive to the distribution of the noise samples and

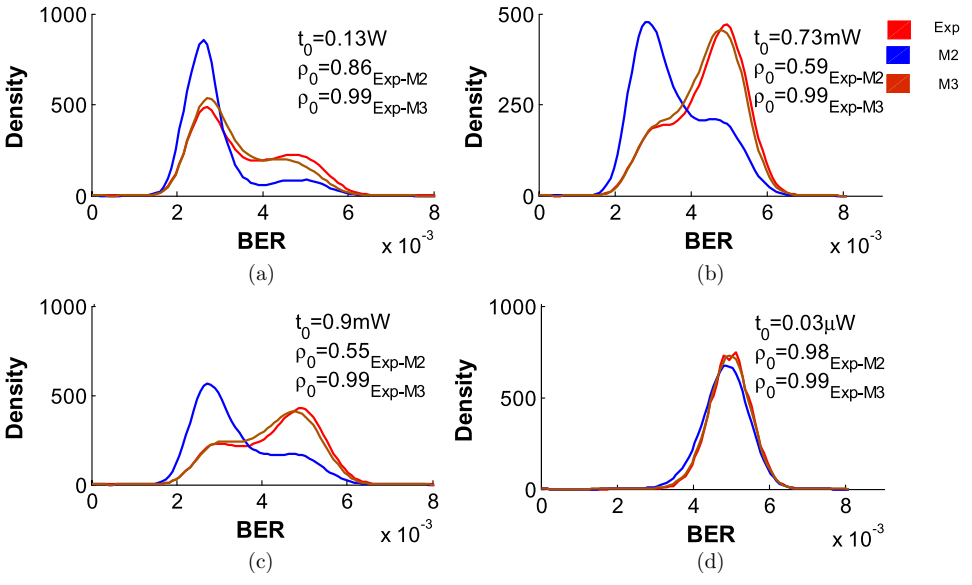

Fig. 11. The probability distributions of BER of OFDMA for different transmit powers in *Site* 2 (LFB) with (t_0, ρ_0) given in the plots.

only a varying PSD does not suffice to emulate the noise successfully. It is also seen from Fig. 10 that ρ_0 is high throughout the range of t_0 in the Exp–M3 distribution even for intermediate powers and better compared to the Exp–M2 case. Table 6 gives the minimum and average ρ_0 for all the bands and sites considering the whole range of t_0. The minimum is found to be as low as 0.1725 for the Exp–M2 distributions whereas the correlation is found to be as high as 0.6730 for Exp–M3 distributions. In the HFB the minimum is found to be 0.2441 against 0.6910. The average ρ_0 over all t_0 is found to be minimum at *Site* 3 (0.6837 against 0.9855) and *Site* 1 (0.6758 against 0.8692) in the two bands, respectively. This shows that the

Table 6. The minimum and average correlation coefficients of the distributions of BER of OFDMA at different transmit powers using the experimental, simulated (Exp–M2 and Exp–M3) and emulated (Exp–$M2_{DAQ}$ and Exp–$M3_{DAQ}$) noises.

Parameters		*Site* 1		*Site* 2		*Site* 3	
		Min ρ	Av ρ	Min ρ	Av ρ	Min ρ	Av ρ
Low frequency	Exp–M2	0.8875	0.9781	0.5524	0.8253	0.1725	0.6837
	Exp–M3	0.9905	0.9982	0.9856	0.9956	0.6730	0.9855
	Exp–$M2_{DAQ}$	0.7440	0.8880	0.4246	0.9453	0.2944	0.8098
	Exp–$M3_{DAQ}$	0.9341	0.9747	0.8564	0.9688	0.8097	0.9495
High frequency	Exp–M2	0.2441	0.6758	0.3006	0.6793	0.5190	0.6865
	Exp–M3	0.6910	0.8692	0.7950	0.9057	0.9159	0.9820

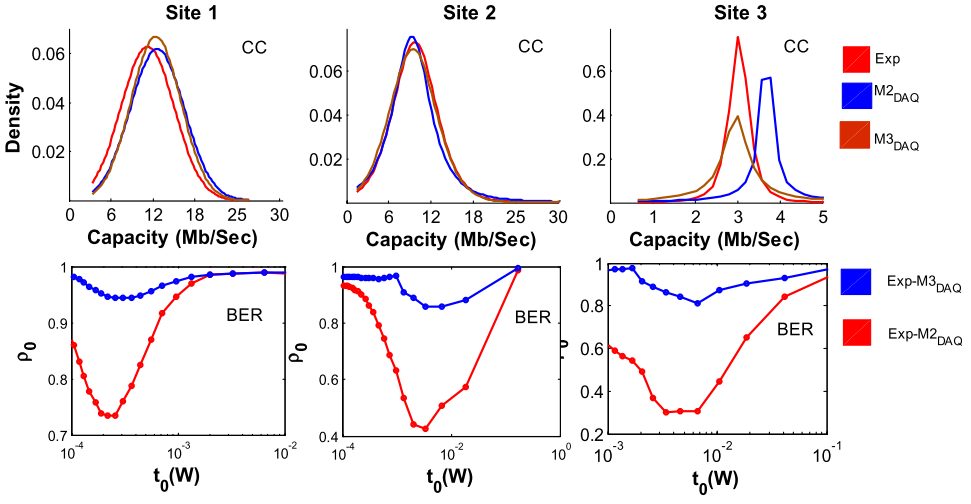

Fig. 12. The plots of the probability density of CC and (t_0, ρ_0) of BER of OFDM in the three sites in the LFB using noise from the DAQ.

M3, which takes into account the PSD and PD of the target, gives a better reflection of the noise statistics.

5.2.3. *Hardware emulation of CBGN*

The hardware for emulation is a 16-bit multifunction DAQ (NI-USB 6251, 1.25 MS/s) operated through LabVIEW software. The simulated noise in the LFB using both M2 and M3 is logged out through the DAC of the DAQ and recaptured by a DSO (Fig. 1). The noises produced are termed as $M2_{DAQ}$ and $M3_{DAQ}$, respectively, and serve as a noise bank for statistical analysis. The PSD of the samples is remodeled and the CC is estimated at the maximum transmit power of the band. Figure 12 shows the distributions of CC in the emulated and experimentally observed noises. The BER of OFDM is also found out in the recaptured noise. The correlation coefficients ρ_0 for the nonparametric distributions of Exp–$M2_{DAQ}$ and Exp–$M3_{DAQ}$ at every transmit power t_0 are plotted in the figure as before. Tables 5 and 6 show the mean and the standard deviation values of CC for all the sites and the average and minimum ρ_0 for the BER, respectively. It is seen from the figure that the distribution of CC is nearly similar. The minimum percentage errors of the mean and standard deviation are found to be 13.12% and 0.31% using $M2_{DAQ}$ and 3.1% and 2.08% using $M3_{DAQ}$ are, respectively. The (t_0, ρ_0) graph also shows high correlation for the Exp–$M3_{DAQ}$ case throughout t_0 compared to the Exp–$M2_{DAQ}$ case. The minimum is found to be as low as 0.2944 for the Exp–$M2_{DAQ}$ distributions whereas the correlation is found to be as high as 0.8097 for the Exp–$M3_{DAQ}$ distributions. The average correlation is also high for $M3_{DAQ}$ compared to $M2_{DAQ}$.

6. Results

Considering all the sites, in Table 5, the average percentage error of the mean of the CC is found to be 11.78% for M2 and 12.68% for M3 in the LFB. The noise emulated using the DAQ has 17.93% and 11.82% deviations using $M2_{DAQ}$ and $M3_{DAQ}$, respectively. For HFB, the average percentage errors are 12.34–10.66% for M2 and M3, respectively. From Table 6, the Exp–M2 distributions showed an average minimum correlation of 0.422 which is far below that of Exp–M3 (0.883). Similarly for the DAQ, it is as small as 0.498 (for Exp–$M2_{DAQ}$) against 0.867 (for Exp–$M3_{DAQ}$). For HFB, the correlation is 0.355 (Exp–M2) against 0.801 (Exp–M3). M3 can therefore provide a better regeneration of the experimental noise within an error limit compared to M1 or M2. The reason for the error is the fitting of the parameters is not completely perfect and the distribution with the minimum KS statistics is only taken. For those parameters for which this technique is difficult to use, other methods such as acceptance–rejection method of generating random numbers can also be used. The simulation of BER of OFDMA shows the importance of simulating a target observed PD instead of the Gaussian noise for noise regeneration. Moreover, in M3, a maximum of 17 parameters (14 for varying PSD and three for target PD as seen in the HFB of *Site* 3) are sufficient to regenerate the statistics of the experimentally observed noise. This is an added advantage over SAM where the parameters at every frequency interval need to be stored for regeneration.

7. Conclusion

The paper presents a method to simulate the observed time-variant CBGN at any site in the indoor PL channels such that the time-domain characteristics are captured by a varying PSD model and the noise amplitude by a target distribution within a limit of error. The emulation is done using a smaller number of parameters compared to the available method namely the SAM. The estimated communication parameters using the emulated noise show close agreement with those obtained with the experimental noise. The method can be used for CBGN generation in the overall noise simulator of PL channels that efficiently portrays the channel behavior. Such a simulator will successfully predict the efficiencies of devices before implementing in actual hardware. Emulating the statistical properties of noise in PL channels will enable development of suitable hardware that can be aimed to be more robust and competent with other networking options.

Acknowledgments

The authors are grateful to the University Grants Commission (UGC) and the Department of Science and Technology (DST), through the FIST program, for providing funds for purchasing the equipment necessary for the study.

References

1. S. Galli, A. Scaglione and Z. Wang, For the grid and through the grid: The role of power line communications in the smart grid, *Proc. IEEE* **99** (2011) 998–1028, doi: 10.1109/JPROC.2011.2109670.
2. B. Tiru, Exploiting power line for communication purpose: Features and prospects of power line communication, *Intelligent Applications for Heterogeneous System Modeling and Design* (IGI Global, 2015), pp. 320–334.
3. S. Chaterjee, B. Tiru, R. Baishya, K. Khan and P. Sarmah, Characteristics of vissible light communication using light-emitting diodes, *Proc. Int. Conf. Computing and Communication Systems*, Lecture Notes in Networks and Systems, Vol. 24 (Springer, 2017), pp. 505–513.
4. E. Biglieri and P. di Torino, Coding and modulation for a horible channel, *IEEE Commun. Mag.* **41** (2003) 92–98.
5. Y. Chen and T. Chiueh, Baseband transceiver design of a 128-kbps power-line modem for household applications, *IEEE Trans. Power Deliv.* **17** (2002) 338–344.
6. M. Zimmermann and K. Dostert, Analysis and modeling of impulsive noise in broad-band powerline communications, *IEEE Trans. Electromagn. Compat.* **44** (2002) 249–258.
7. A. G. Lazaropoulos, The impact of noise models on capacity performance of distribution broadband over power lines networks, *J. Comput. Netw. Commun.* **2016** (2016) 5680850.
8. T. Esmailian, F. R. Kschischang and P. G. Gulak, Characterization of in-building power lines at high frequencies and their channel capacity, *Proc. IEEE Int. Symp. Power Line Communications and its Applications* (2000), pp. 52–59.
9. B. Tiru and P. K. Boruah, Multipath effects and adaptive transmission in presence of indoor power line background noise, *Int. J. Commun. Syst.* **23** (2010) 63–67, doi: 10.1002/dac.1044.
10. R. Baishya, B. Tiru, S. Chatterjee, K. Gogoi and U. Sarma, Time dependent indoor power line background noise: Analysis, simulation and effect on communication system, *Proc. 2016 Int. Conf. Advances in Electrical, Electronic and Systems Engineering* (2016), pp. 231–235.
11. H. Meng, Y. L. Guan and S. Chen, Modeling and analysis of noise effects on broadband power-line communications, *IEEE Trans. Power Deliv.* **20** (2005) 630–637, doi: 10.1109/TPWRD.2005.844349.
12. N. Andreadou and F. N. Pavlidou, Modeling the noise on the OFDM power-line communications system, *IEEE Trans. Power Deliv.* **25** (2010) 150–157, doi: 10.1109/TPWRD.2009.2035295.
13. A. H. Najarkolaei, W. Hosny and J. Lota, Bit error rate performance in power line communication channels with impulsive noise, *Proc. 2015 17th UKSim-AMSS Int. Conf. Modelling and Simulation* (2015), pp. 248–251.
14. S. Sancha, F. J. Cantete and J. T. Entrambasaguas, A channel simulator for indoor power-line communications, *Proc. 2007 IEEE Int. Symp. Power Line Communications and Its Applications* (2007), pp. 104–109, doi: 10.1109/ISPLC.2007.371106.
15. F. J. Canete Corripio, L. Diez del Rio and J. T. Entrarnbasaguas Munoz, A time variant model for indoor power-line channels, *Proc. Int. Symp. Power Line Communications and Its Applications* (2001), pp. 85–90.
16. H. Phillips, Modelling of powerline communication channels, *Proc. 3rd Int. Symp. Powerline Communications and Its Applications* (1999), pp. 14–21.
17. L. D. Bert, P. Caldera, D. Schwingshack and A. M. Tonello, On noise modeling for power line communications, *Proc. 2011 IEEE Int. Symp. Power Line Communications and Its Applications* (2011), pp. 283–288.

18. D. Benyoucef, A new statistical model of the noise power density spectrum for powerline communication, *Proc. 7th Int. Symp. Power Line Communications and Its Applications* (2003), pp. 136–141.
19. M. Nassar, A. Dabak, I. Kim, T. Pande and B. Evans, Cyclostationary noise modeling in narrowband powerline communication for smart grid application, *Proc. IEEE Int. Conf. Acoustics, Speech and Signal Processing* (2012), pp. 3089–3092.
20. Y. Xiao, J. Zhang, F. Pan and Y. Shen, Power line communication simulation considering cyclostationary noise for metering systems, *J. Circuits Syst. Comput.* **25** (2016) 1650105-1–1650105-13, doi: 10.1142/S021812661650105X.
21. A. Voglgsang, T. Langguth, G. Korner and H. Steckenbiller, Measurement characterization and simulation of noise on powerline channels, *Proc. Int. Symp. Power Line Communications and Its Applications* (2000), pp. 139–146.
22. K. Dostert, M. Zimmermann, T. Waldeck and M. Arzberger, Fundamental properties of the low voltage power distribution grid used as data channel, *Eur. Trans. Telecommun.* **11** (2000) 297–306.
23. A. G. Burr, D. M. W. Reed and P. A. Brown, Effect of HF broadcast interference on power line telecommunications above 1 MHz, *Proc. IEEE GLOBECOM* (1998), pp. 2870–2875.
24. O. G. Hooijen, On the channel capacity of the residential power circuit used as a digital communications medium, *IEEE Commun. Lett.* **2** (1998) 267–268, doi: 10.1109/ISIT.1997.613404.
25. J. Meng, Noise analysis of power-line communications using spread-spectrum modulation, *IEEE Trans. Power Deliv.* **22** (2007) 1470–1476, doi: 10.1109/TPWRD.2007.900301.
26. A. D. Spaulding and D. Middleton, Optimum reception in an impulsive interference environment — Part I: Coherent detection, *IEEE Trans. Commun.* **25** (1977) 910–923, doi: 10.1109/TCOM.1977.1093943.
27. L. Wei, Z. Xue and Q. Liu, Research and software implementation on PLC channels simulation system based on FPGA, *Proc. 2015 Int. Conf. Intelligent Systems Research and Mechatronics Engineering* (2015), pp. 632–637.
28. K. R. Gurley, Modelling and simulation of non-Gaussian processes, Ph.D. Thesis, University of Notre Dame (1997), https://www3.nd.edu/∼nathaz/journals/Dissertation_Gurley.pdf.
29. F. Yamazaki and M. Shinozuka, Digital generation of non-Gaussian stochastic fields, *J. Eng. Mech.* **114** (1988) 1183–1187.
30. E. Y. Matsumoto and E. Del-Moral-Hernandez, Using neural networks committee machines to improve outcome prediction assessment in nonlinear regression, *Proc. Int. Joint Conf. Neural Networks* (2013).
31. J. G. Proakis and D. G. Manolakis, *Digital Signal Processing: Principles, Algorithms and Applications* (Prentice-Hall, New Delhi, 2009), Chapter: Design of Digital Filter, p. 671.
32. R. C. Galleger, *Information Theory and Reliable Communication* (John Wiley & Sons, New York, 1986), Chapter: Waveform Channels, p. 389.
33. O. G. Hooijen and A. J. H. Vinck, On the channel capacity of a European-style residential power circuit, *Proc. 1998 Int. Symp. Power Line Communication* (1998), pp. 229–237.
34. J. van Wyk and L. Linde, Bit error probability of M-ary QAM OFDM-based system, *Proc. 2007 IEEE AFRICON* (2007), pp. 1–5.